AIAA-2003-0607
Compound Aircraft Transport: A Comparison of Wingtip-Docked and Close-Formation Flight

S. A. Magill, J.A. Schetz and W.H. Mason
Virginia Polytechnic Institute and State University
Blacksburg, VA

41st AIAA Aerospace Sciences Meeting & Exhibit
6-9 January 2003 / Reno, NV

AIAA 2003-0607

COMPOUND AIRCRAFT TRANSPORT: A COMPARISON OF WINGTIP-DOCKED AND CLOSE-FORMATION FLIGHT

Samantha A. Magill,*
Joseph A. Schetz†
and William H. Mason‡

Virginia Polytechnic Institute & State University
Blacksburg, Virginia

Abstract

Compound Aircraft Transport (CAT) flight involves two or more aircraft using the resources of each other; a symbiotic relationship exists consisting of a host, the *mothership* aircraft and a parasite, the *hitchhiker* aircraft. Wingtip-docked flight is just as its name implies; the two aircraft are connected wingtip-to-wingtip. Formation flight describes multiple aircraft or flying objects that maintain a pattern or shape in the air. There are large aerodynamic advantages in CAT flight. Wingtip-docked flight increases the total span of the aircraft system, and formation flight utilizes the upwash from the trailing wingtip vortex of the lead aircraft to reduce the energy necessary to achieve and/or maintain a specific flight goal for the system.

The Stability Wind Tunnel at Virginia Tech, computational aerodynamic analysis with the vortex lattice method (VLM), and a desktop aircraft model were used to study questions of the best location for a hitchhiker aircraft in a CAT system. Wind tunnel tests implemented a 1/32 scale F-84E model (hitchhiker) and an outboard wing portion representing the B-36 (mothership). These models were chosen to simulate flight tests of an actual wingtip-docked project, *Tom Tom*, in the 1950s. The wind tunnel test included a broad range of hitchhiker locations: varying spanwise gap distance, longitudinal or streamwise distance, and vertical location (above or below wing) with respect to a B-36-like wing. The data showed very little change in the aerodynamic forces of the mothership, and possibilities of large benefits in lift and drag for the hitchhiker when located slightly aft and inboard with respect to the mothership. Three CAT flight configurations were highlighted: wingtip-docked, close formation, and towed formation. The wingtip-docked configuration had a 20–40% performance benefit for the hitchhiker compared to solo flight. The close-formation configuration had L/D performance benefits for the hitchhiker approximately 10 times that of solo flight, and the towed formation was approximately 8 times better than solo flight.

The VLM analysis completed and reinforced the experimental wind tunnel data. A modified VLM program (VLM CAT) incorporated multiple aircraft in various locations as well as additional calculations for induced drag. VLM CAT results clearly followed the trends seen in the wind tunnel data, but since this VLM implementation did not model the fuselage, and assumed a flat wake, and is an inviscid computation it did not predict the large benefits or excursions as seen in the wind tunnel data. Increases in L/D performance for the hitchhiker in VLM CAT were on the order of 3 to 4 times that of the hitchhiker in solo flight, while the wind tunnel study saw up to 10 times that of solo flight. VLM CAT is a valuable tool in supplying quick analysis of position and planform effects in CAT flight.

The aerodynamic results presented in this study have determined some important parameters in the location of a hitchhiker with respect to a mothership. The largest aerodynamic benefits are seen when the hitchhiker wingtip is slightly aft, inboard and below the wingtip of the mothership.

*Graduate Assistant now at AeroVironment, Inc.

†Fred D. Durham Chair, Department of Aerospace & Ocean Engineering, Fellow AIAA

‡Professor Department of Aerospace & Ocean Engineering, Associate Fellow AIAA.

Wind Tunnel Tests

Wind tunnel tests were conducted using models representing the aircraft and conditions in the *Tom Tom* Project of the 1950's[123]. The goal was to measure forces and the moments on two models representing the mothership (MS) and the hitchhiker (HH), and to record flow visualization of the trailing vortex interaction. The models were a retail-bought 1/32 scale F-84E, *Thunderstreak*, for the hitchhiker and an in-house manufactured composite wing to represent the outboard wing-section of the B-36, *Peacemaker*, the transport wing, for the mothership.

Experimental Setup

The tests were conducted in the Stability Wind Tunnel of Virginia Tech with a test section 6' X 6' X 24'. The swept-wing F-84 and transport wing configuration was setup vertically in the test section using the tunnel floor as a plane of symmetry. 1 is an example of the general test setup. Representing only the outer portion of the B-36 wing (transport wing) minimized construction time and allowed for a higher Reynolds number. Also, boundary layer trip strips were adhered to each lifting surface, thus ensuring a simulation of a reasonable flight Reynolds number.

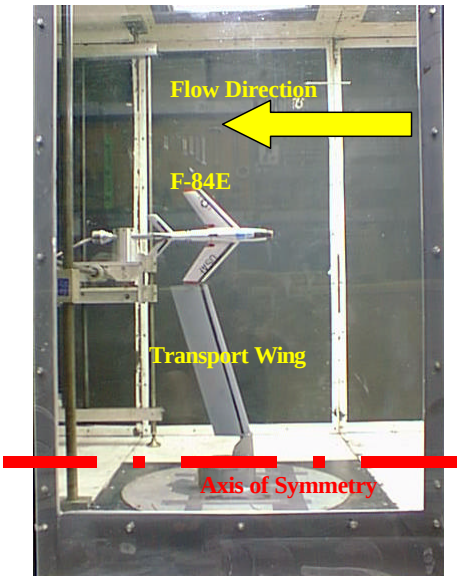

Figure 1: Wind Tunnel Testing Setup

The F-84 model with an internal sting balance was mounted on a traverse mechanism that is mobilized by a stepper motor and has vertical and horizontal motion in a cross-sectional plane perpendicular to the streamwise flow.

Table 1 gives a comparison of the full-scale and sub-scale wind tunnel models. The swept-wing variant 1/32 scale F-84E has a wing span of 12.5 inches. The *Tom Tom* Project of the 1950s employed an F-84F; the F-84E is only differentiated from the F-84F by the propulsive changes not geometric changes.

The transport wing (TW) model was built specifically for these tests. It had comparable B-36-to-F-84 ratios of tipchord, and a similar leading edge sweep and wingtip airfoil shape of the B-36. The instrumentation setup and data acquisition system is described in Magill[4].

Table 1: Comparison of Wind Tunnel Model Scale to Actual Scale

	TW	**B-36**	**F-84E Model**	**F-84F**
c_{tip}	5.0 in	21.0 ft	2.4 in	6.25 ft
AR	4.0	11.1	4.26	4.72
Λ_{LE}	$15.^o$	$15.^o 6.5'$	$45.^o$	$45.^o$
Airfoil	63–420[1]	63(420)–517[1]	HSL[2]	HSL[2]

Coordinate System

The orthogonal coordinate system (x, y, and z) used in testing was nondimensionalized by the average chord of the F-84E model ($c_{ave} = \frac{c_{root}+c_{tip}}{2} =$ 2.94 inches). The nondimensional coordinate system was defined with Greek notation, (ξ, η, ζ).

The angle of attack, α, roll, ϕ, and sideslip angle, β, followed the standard aircraft definition for these angles throughout this study. Figure 2 shows the coordinate system and angle definitions, respectively.

Experimental Procedures Conditions and Configurations

The testing consisted of force and moment measurements focusing on the changes seen by the F-84 model, and flow visualization of the trailing vortex interaction between the F-84 and transport wing. All measurements were taken at a tunnel dynamic pressure, $q = 4.5$ inches of water ($\sim$ 100 mph), and all flow visualization was performed at a lower tunnel speed, $q = 1.5$ inches of water so as not to lose the tufts.

The CAT configurations were tested at various angle of attack and sideslip angle combinations. The

[1]NACA Airfoil
[2]High Speed Laminar Airfoil

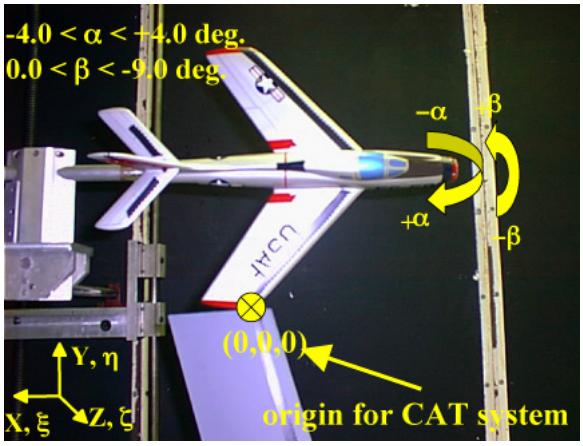

Figure 2: Wind Tunnel Angle and Orthogonal Coordinates, for Wind Tunnel Configuration One: *Wingtip-Docked CAT Flight*

angles chosen were constrained by the mechanical setup seen in the left of Figure 2, that were approximately -6, -4, 0, +4, +6 degrees for angle of attack and +9, +2.5, 0, -2.5, 9 degrees for sideslip angle. The angle of attack was measured with respect to the F-84 fuselage centerline or longitudinal plane of symmetry referenced to the tunnel walls, and sideslip angle was measured with respect to the F-84 or lateral plane of symmetry referenced to the tunnel floor. Due to the difficultly in accurately measuring angle of attack, measured C_L is employed as a distinguishing reference condition for all configurations. The testing consisted of a broad scope of parameters and configurations that relied on the flow visualization to define the areas of importance. Only three of the six configurations are presented here for comparison to the computational analysis; for data at other configurations see Magill[4].

Configuration One: *Wingtip-Docked CAT Flight* The first test configuration started with the origin or zero location of the F-84-wingtip-quarter-chord to transport-wingtip-quarter-chord. The F-84 was moved in the negative ζ-direction, which is below the transport wing, and in the negative η-direction, which is toward the transport wingtip as if coming up and in for docking. The $\eta \times \zeta$ grid was 2×1 inches square. The angle of attack and sideslip variations were approximately -4, 0, +4 degrees and 0, -2.5, -9 degrees, respectively. α variation corresponds to a C_L = -0.03, 0.48, 0.98, respectively.

Configuration Two: *Close Formation CAT Flight*

The second test configuration was set up with one transport wing chordlength (5.0 inches) separation between the trailing edge of the TW and the leading edge of the F-84 model ($\xi = 3.0$). This was termed close formation flight, because the hitchhiker takes advantage of the mothership trailing vortex upwash while still maintaining the possibility of being rigidly connected to the mothership. This arrangement can also utilize the energy savings of docked or carried flight by flying at conditions of minimal power: engines off or ideal. The tests employed the same pitch and yaw combinations as the first test configuration, and the zero location was in the F-84 model wingtip-to-transport wingtip plane as seen in Figure 3. This is the same zero-plane as that in configuration one. The F-84 was now capable of moving inboard of the transport wingtip one inch, and the grid was also expanded to include positive ζ. The $\eta \times \zeta$ grid was 2×4 inches square.

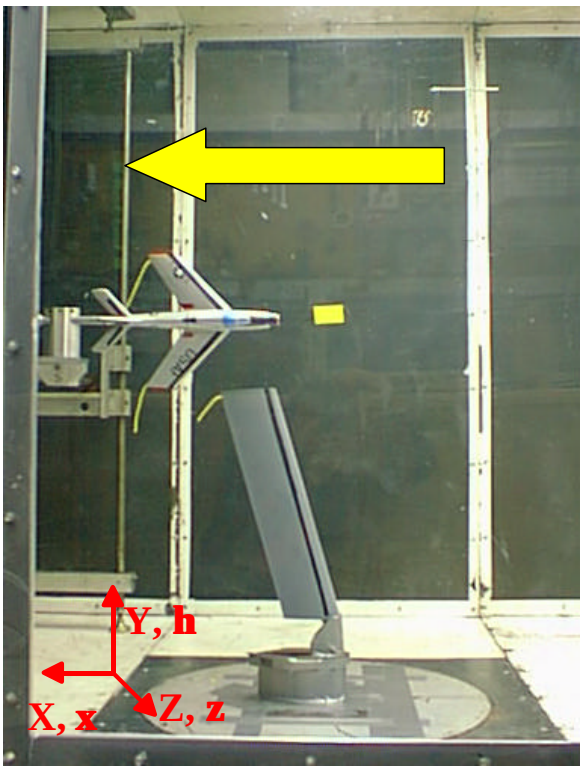

Figure 3: Testing f : *Close Formation CAT Flight* (No flow: tufts hanging down)

Configuration Five: *Towed Formation CAT Flight* The fifth test configuration attempted to simulate towed formation flight by moving the nose

of the F-84 back 15 inches or $\xi = 10.0$ (three chordlengths of the transport wing) from the trailing edge of the transport wing. In this configuration, the hitchhiker could be connected to the mothership by a tether or unconnected maintaining flight in the mothership trailing vortex manually or through automation. A traverse was made though the flow field in the plane perpendicular to the free-stream or $\xi - \zeta$ plane, the F-84 nose in-plane with the transport wingtip, recording force and moment measurements, as well as flow visualization. Figure 4 shows the setup.

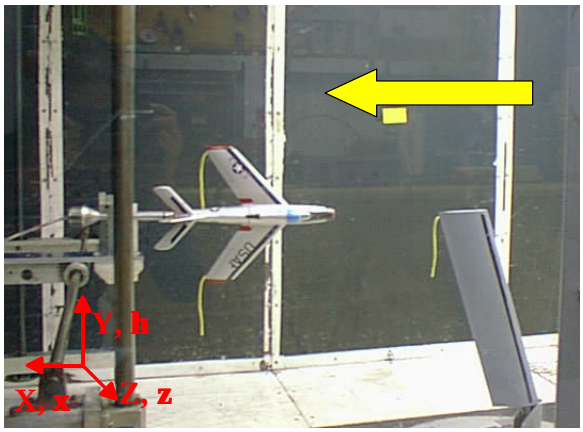

Figure 4: Testing Configuration Five: *Towed Formation CAT Flight* (No flow: tufts hanging down)

Wind Tunnel Results

The data for the F-84 model at an approximately zero degree sideslip and angle of attack is presented in this section, and complementary data for other sideslip angles is located in Magill[4].

The plots show data in terms of standard nondimensional aerodynamic coefficients based on the free-stream conditions and planform geometry of the F-84 model for lift (C_L), drag (C_D), rolling moment(C_l), and lift-to-drag ($(L/D)/(L/D)_{solo}$) ratio versus spanwise location, η, of the F-84 model for several vertical locations above and below the transport wing, ζ. $()_{solo}$ denotes a value for the F-84 model (or transport wing) when the two models are far removed, from each. Each vertical or ζ position has a symbol that is constant for all the plotted wind tunnel data. For example when the F-84 model and transport wing are in the spanwise-plane, this is the zero ζ location represented with the $*$'s. If the F-84 model is above the transport wing, then ζ is positive above and is negative below. For a positive ζ, the symbols are open, and for negative ζ, the symbols are closed, but the symbol for the absolute value of ζ is the same.

The data is best analyzed through the lift-to-drag ratio. Lift and drag are coupled in determining maximum aerodynamic performance. Viewing only one as a benefit determiner, while the other may be subject to adverse effects, leads to an inaccurate study of the system. A comparison between the aircraft in *solo* flight to the aircraft in CAT flight is important in determining the overall benefits of CAT flight, therefore a lift-to-drag ratio between CAT and solo flight is defined, $(L/D)/(L/D)_{solo}$. L/D without a subscript represents the ratio for the configuration tested. The solo values were determined through asymptotic estimation as the F-84 model is moved away from the transport wing, and are $L/D \approx 18$, and $C_L \approx 0.49$ for the F-84 model.

Rolling moment coefficient is also presented because of control surface deflection limitations in maintaining level or trimmed flight in a strong vortex field.

Flow Visualization

The interesting thing to note in the flow visualization videos is how the smaller trailing vortex from the F-84 is sucked into the more powerful vortex of the transport wing, which appears to be unaffected by the smaller aircraft. The left (farside) wingtip vortex of the F-84 model generally did not appear to be affected by the transport wingtip vortex in any configuration. A more detailed description of this data is presented in Magill[4].

Configuration One: *Wingtip-Docked CAT Flight*

The arrangement is shown in Figure 2 and again the results are presented in terms of forces and moments on the F-84 model versus spanwise distance, η, for several vertical locations above and below the transport wing, ζ. Figures 5 through 8 give the data for lift, drag, and rolling moment coefficient as well as the $(L/D)/(L/D)_{solo}$ ratio defined previously.

In Figure 5, the F-84 closes the spanwise distance between it and the transport wingtip from an $\eta = 0.68$ to an $\eta = 0.0$ ($\eta = 0.0$ being a wingtip-docked position). The lift first increases gradually and then more rapidly beginning at an $\eta \approx 0.3$ and $C_L \approx 0.55$. At $\eta = 0.0$ the span between the F-84 and transport wing would be continuous, and that, as theory predicts, is the point of maximum lift, $C_{L_{max}} \approx 0.59$. Figure 5 also shows data for

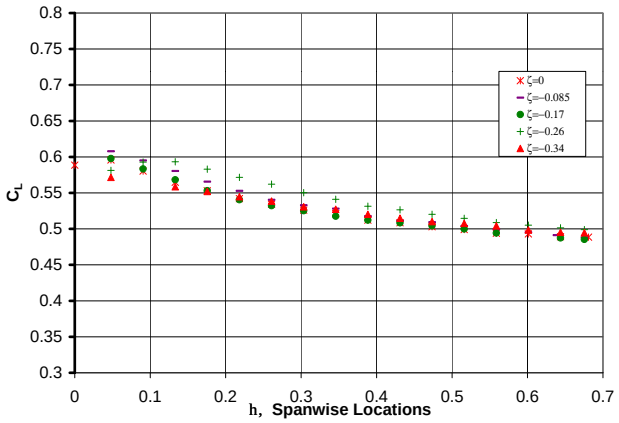

Figure 5: C_L vs. η, Spanwise Distance for Configuration One

several vertical locations, ζ, of the F-84 model with respect to the transport wing. A hitchhiker aircraft docking to a mothership would approach from below, so to simulate this docking procedure only the vertical positions of the F-84 model below the transport wing, $-\zeta$, were tested. The $*$'s represent the zero vertical location where the F-84 model and transport wing are in the same spanwise-plane, $\zeta = 0.0$. The data for all vertical locations follows the same general trend established by the $\zeta = 0.0$ location. The crosses represent the data for the F-84 at a vertical location of $\zeta = -0.26$, only 26% of the F-84 model average chord (2.94 inches). This relatively small negative ζ value yields an overall increase in lift compared to the other ζ positions.

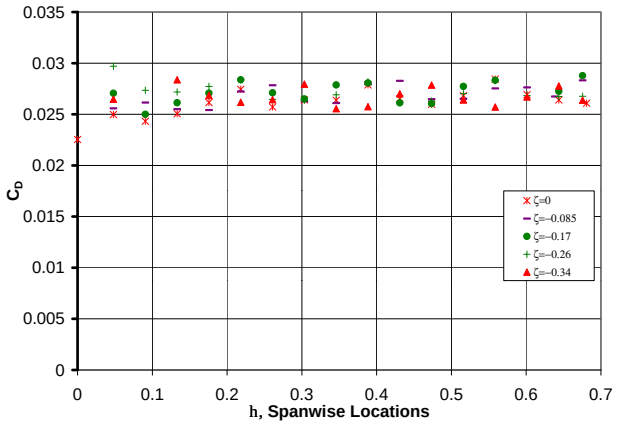

Figure 6: C_D vs. η, Spanwise Distance for Configuration One

The drag data in Figure 6 is quite invariant as the F-84 model moves from $\eta = 0.68$ to $\eta = 0.0$, closing in on the transport wing for a docked position. The drag of the F-84 model is banded averaging approximately $C_D \approx 0.27$. There is no vertical, ζ, or spanwise η location of distinguishable advantage in consistently minimizing drag.

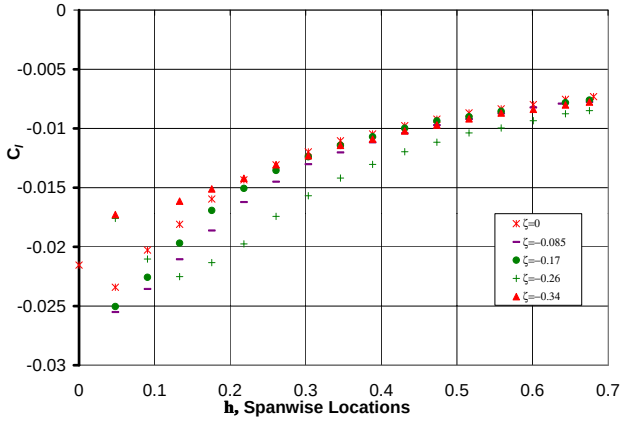

Figure 7: C_l vs. η, Spanwise Distance for Configuration One

The magnitude of rolling moment in Figure 7 increases as the F-84 moves spanwise in to a docked position. This should be intuitive to the reader due to the clockwise rotation for the left wingtip vortex of the transport wing. The air flow must circulate from the high pressure region (lower surface) to the low pressure region (upper surface), thus an upwash is hitting the inboard wing (or right wing) of the F-84 model. The changes in rolling moment occur quicker than the changes in lift in Figure 5. But like the variation in lift, the magnitude of the rolling moment begins to increase very rapidly approximately an $\eta = 0.3$ and $C_l \approx -0.013$. Also like the lift data in Figure 5, the $+$'s that correspond to a vertical position, $\zeta = -0.26$, of the F-84 model below the transport wing have the greatest increase in roll. The data for the two vertical positions furthest below the transport wing, the crosses, $\zeta = -0.26$, and the triangles, $\zeta = -0.34$, deviate from the general path at an $\eta \approx -0.1$. The rolling moment data decreases in magnitude for those two points. Perhaps the right wing of the F-84 model is coming into contact with the downwash of the transport wingtip vortex or is moving out of the influence region. The maximum rolling moment seen is at an $\eta \approx 0.0$, wingtips aligned, $C_l = -0.025$. The negative sense of rolling moment variation is based on the standard aircraft coordinate system; the up-

wash of the transport wingtip vortex is impacting the inboard or right wing of the F-84 model, thus the F-84 is rolling counterclockwise (left wingtip down) and that is defined as negative rolling moment. The trends in magnitude between lift and rolling moment coincide, but though increases in lift are beneficial, the increases in rolling moment are not. It is the zero vertical position for the F-84 model, the $*$'s, $\zeta = 0.0$, that shows the least variation in rolling moment compared to the non-zero vertical positions. Ideally, rolling moment should equal zero far away, where a trimmed flight condition exists. If the aircraft could not be trimmed (i.e. not deflect the control surfaces enough), the pilot might lose control or become fatigued trying to stay straight and level. So, the large benefits in lift for a docked position as seen in Figure 5 may not be reasonable to achieve, because of the difficulty to maintain trimmed flight.

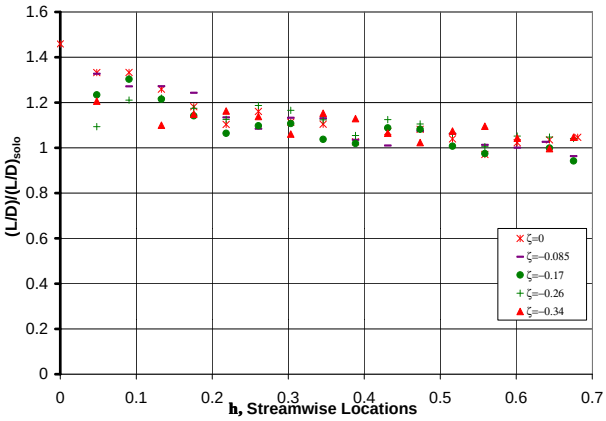

Figure 8: L/D vs. η, Spanwise Distance for Configuration One

Figure 8 plots the L/D data for the F-84 model as a ratio to the solo value of L/D. Since the drag is fairly constant in Figure 6, and the lift increases as the F-84 moves toward the transport wingtip in Figure 5, the increase of L/D in Figure 8 is logical. The L/D data shows no distinguishing advantage in a vertical position, ζ, for the F-84 model. The zero vertical position, the $*$'s, $\zeta = 0.0$, at $\eta = 0.0$ or wingtips-docked has the highest $(L/D)/(L/D)_{solo}$ value at ≈ 1.45. As mentioned earlier, L/D is viewed as the determining flight performance parameter, thus Figure 8 is the most important in determining the benefits of this flight configuration compared to solo flight. This benefit for wingtip-docked flight is shown as an approximate 20%–40% increase in performance.

Configuration Two: *Close Formation CAT Flight*

For this configuration the F-84 model is moved downstream slightly to an $\xi = 3.0$ as in Figure 3. Figures 9 through 12 give the data for this configuration, and it is presented like the data for Configuration One, previously; lift, drag, roll and L/D, plotted versus the spanwise gap, η, between the F-84 model and the transport wing for various locations of the F-84 model above and below the transport wing. For clarity, the location of the wingtip-to-wingtip plane is highlighted by a bold line along the vertical axis at $\eta = 0.0$. The vertical positions above and below the transport wing, ζ, cover a broader range than that for Configuration One, now including positive values of ζ with the F-84 model moving above the transport wing. Positive values of ζ are represented as open symbols, while the mirrored negative ζ values are represented as a closed symbol.

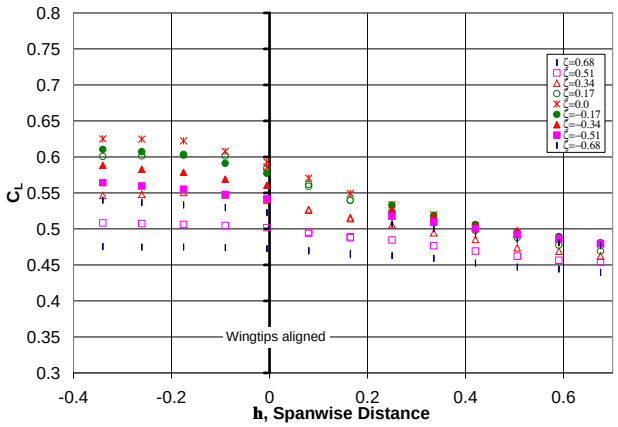

Figure 9: C_L vs. η, Spanwise Distance for Configuration Two

The lift data in Figure 9 increases as the F-84 is moved in and continues to increase as the F-84 wingtip moves inboard of the transport wingtip, $-\eta$. The lowest η value is -0.34, 34% of the average chord for the F-84 model, only 8% of the F-84 span and 5% of the transport wing span. This is a relatively small distance. A position for the F-84 model wingtip slightly inboard of the transport wingtip means that more of the F-84 is enveloped in the upwash of the transport wing; it is well known that the core of a wingtip vortex rolls-up slightly inboard of the wingtip. If the F-84 moves further inboard of the transport wingtip, the downwash would begin to contribute negatively to the lift of the F-84.

This switch to a downwash region is evident in Figure 9 with the introduction of a levelling-off or peak in the lift at $\eta \approx -0.2$.

The variation in lift for different vertical locations, ζ, fans out as the F-84 model nears the transport wingtip and continues to do so inboard of the wingtip. The fanning or spreading out of the lift data for $\eta < 0.25$ can be attributed to the F-84 contact with the transport wingtip vortex, which has begun to diffuse radially. A radial diffusion would create a larger region of influence for the transport wingtip vortex to act on the F-84, thus the fanned out lift data compared to the wingtip-docked lift data. This fanning pattern is carried throughout the close formation data.

The lift data for $\eta = \zeta = 0.0$ in Figure 9 is more or less identical corresponding to the wingtip-docked configuration ($\xi = 0.0$) in Figure 5. Compare the $*$'s in Figure 9 at the wingtip-to-wingtip point, $\eta = 0.0$, (the bold vertical line) with the red $*$'s in Figure 5 at the far left. Also examine, $\eta = 0.0$. The lift values are, for all practical purposes, equal, $C_L \approx 0.60$ on Figure 5, and $C_L \approx 0.59$ on Figure 9. Thus, the lift appears invariant with respect to longitudinal or stagger position.

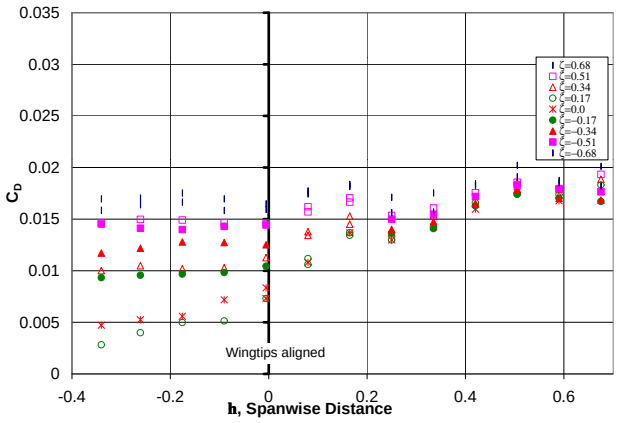

Figure 10: C_D vs. η, Spanwise Distance for Configuration Two

In Figure 10, the drag data, for the F-84 in Configuration Two or *close formation* is presented. Compared to Figure 6 for the wingtip-docked configuration, $\xi = 0.0$, the overall drag has decreased. All data in Figure10 is less than $C_D \approx 0.02$, and in Figure 6 the drag data is banded between $C_D = 0.03$ and $C_D = 0.02$. The maximum for drag in Figure 10 is for a spanwise location for the F-84 at about $\eta = 0.5$ and $C_D = 0.02$, while the minimum is at $\eta = -0.34$ and $C_D \approx 0.005$, very near zero. Upwash can cause a negative induced drag or positive thrust, thus at some point $C_D = 0$.

Whether, in general, above or below the transport wing is more beneficial in drag for the F-84 is not as clear as that for the lift data for Configuration Two. The vertical position data is clustered until the F-84 wingtip passes the transport wingtip, $\eta = 0.0$ (the bold vertical line), and then clearly the $*$'s and ◯'s depart and decrease rapidly. Referring to the legend in Figure 10, the $*$'s are at a zero vertical position for the F-84 model, $\zeta = 0.0$, and the ◯'s are at a vertical position for the F-84 model slightly above the transport wing, $\zeta = 0.17$. Perhaps also worthy of note, the next best vertical position for the F-84 is the mirror of the ◯'s, the closed circles. A conclusion could be drawn that a slightly off-center location for the F-84 is best in terms of drag for close formation flight.

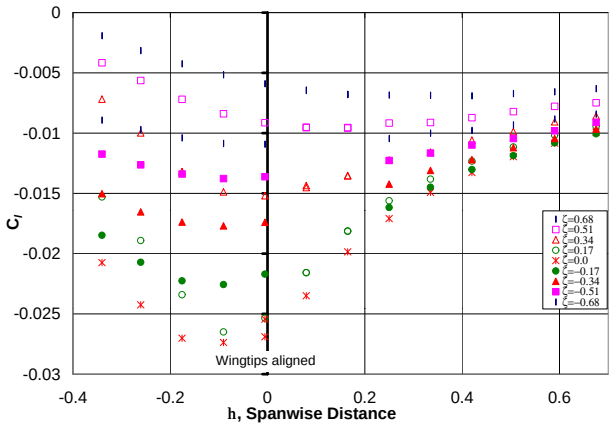

Figure 11: C_l vs. η, Spanwise Distance for Configuration Two

In Figure 11, the trend in rolling moment for the F-84 wingtip outboard of the transport wingtip, $\eta > 0.0$, appears to be similar to that for the wingtip-docked configuration in Figure 7. For both configurations, the magnitude of the rolling moment at the furthest right spanwise position, $\eta = 0.68$, is $C_l \approx 0.005$ increasing as the F-84 model moves toward the transport wing. There is a short continuation of the increasing rolling moment to a maximum magnitude of $C_l \approx 0.027$ and then a decrease or roll reversal tending towards zero. As the F-84 wingtip moves inboard of the transport wingtip, it begins to become subject to the downwash. This would cause the F-84 to roll in the opposite direction, thus the roll data follows the levelling-off or peak in the lift data, Figure 9.

The best vertical position, ζ, for the rolling moment data is furthest away from the transport wing and the disturbances of her wingtip vortex. The best rolling moment value would be zero for trimmed flight, thus expending no extra energy in control surface deflections. The maximum rolling moment is at the vertical position of zero, $\zeta = 0.0$, and the magnitude of rolling moment decreases consistently with increasing vertical separation; following $\eta = 0.0$, the $*$'s, for $\zeta = \pm 0.17$ are the $\bigcirc$'s for $\zeta = \pm 0.34$, and then the $\triangle$'s, and so forth.

The lift and roll data from both Configurations One and Two show a trade-off in flight performance benefits for the F-84 model. To have benefits in lift, the F-84 needs to be close to the transport wingtip vortex, but the least penalty in the rolling moment is to be far away from that vortex.

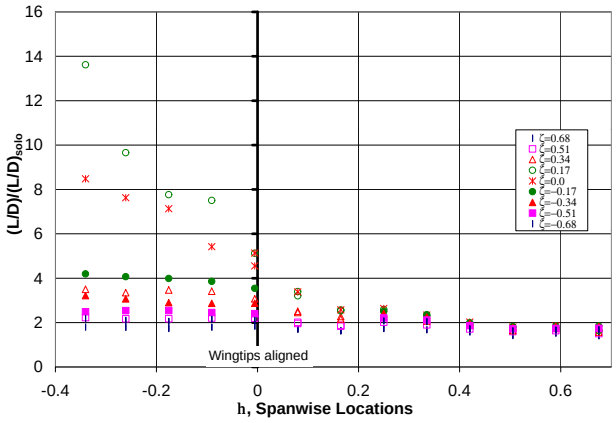

Figure 12: L/D vs. η, Spanwise Distance for Configuration Two

In Figure 12, the L/D data is presented as a ratio, as previously, to the solo L/D value for the F-84. This is plotted versus spanwise separation, η between the F-84 and the fixed transport wing. Compared to the wingtip-docked data in Figure 8, this data for close formation is dramatically more beneficial. As the F-84 moves toward the transport wing, $\eta > 0.0$, the data varies little compared to the variation of the data inboard of the transport wingtip, $\eta < 0.0$. Focusing first on the L/D data for the F-84 model outboard of the transport wingtip, $\eta > 0.0$ or to the right of the bold vertical line, it shows two to three times increase in flight performance compared to that of the wingtip-docked in Figure 8. At the wingtip-docked plane, $\eta = 0.0$, the zero vertical position represented by the $*$'s, $\zeta = 0.0$, $(L/D)/(L/D)_{solo} \approx 4.0$ this corresponds to a 400% increase in flight performance from solo flight of the F-84. As the F-84 wingtip passes inboard of the transport wingtip, $\eta = 0.0$, the majority of the data asymptotically approaches the $(L/D)/(L/D)_{solo}$ value seen at the wingtip-to-wingtip point, $\eta = 0.0$ and $\zeta = 0.0$, which is 4.0, but two of the vertical locations take-off inboard of the transport wingtip. Those two vertical positions happen to correspond with the two decreasing rapidly in the drag data (Figure 10), thus it is evident that the reduction in induced drag is driving the benefits in close formation flight. The beneficial vertical positions are the wingtip-to-wingtip plane, $\zeta = 0.0$ and the vertical plane slightly above the transport wing at $\zeta = 0.17$. The corresponding C_D values in Figure 10 travel very close to zero, and at zero the L/D data would be infinite. This is caused by the upwash of the trailing vortex from the transport wing, and it would be tight and powerful close to the transport wingtip, because dissipative forces have had little time to affect the trailing wingtip vortices. This should explain the large increase in $(L/D)/(L/D)_{solo}$. At the wingtip-to-wingtip plane, $\eta = 0.0$, an $\approx 700\%$ increase from solo flight for the F-84 is seen. And, up to a 1100% increase is seen at the vertical position slightly above the transport wing, $\zeta = 0.17$ and $\eta = -0.34$. Though close formation shows a large benefit aerodynamically to the system, the proximity of the F-84 to the transport wing may be too close for the F-84 to control his position.

Configuration Five: *Towed Formation CAT Flight*

Figures 13 through 16 show the same type of wind tunnel data previously discussed, but now for the towed formation or Configuration Five, which is shown in Figure 4. The F-84 has been moved downstream three chordlengths of the transport wing or five of the F-84 ($\xi = 10.0$). It was set up for a slightly different purpose (towed or tethered flight), thus the focal point was with the F-84 nose aligned transport wingtip. This spanwise position, $\eta = -2.13$, is highlighted with a bold vertical line located about midway on all the plots for this configuration. Also highlighted is the same wingtip-docked plane, $\eta = 0.0$, to the far right of the data. Another note on this towed configuration data is that only data for one vertical position was acquired, that is in the wingtip-docked plane, $\zeta = 0.0$.

In Figure 13, the lift data for the F-84 in towed formation is presented versus spanwise location, η. The data point to the far right of the plot, $\eta = -0.43$

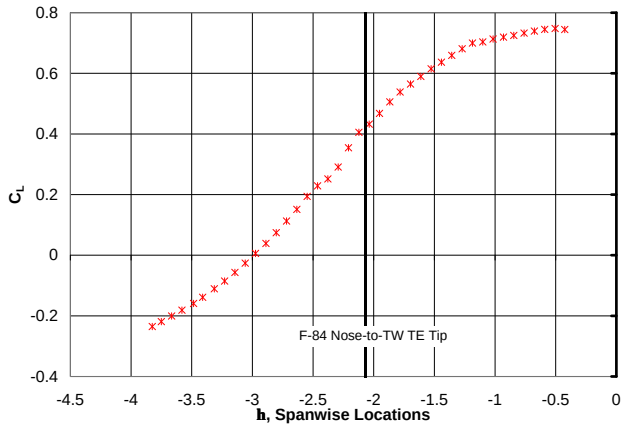

Figure 13: C_L vs. η, Spanwise Distance for Configuration Five

and $C_L \approx 0.77$, is closest for comparison to $\eta = -0.34$, the far left point in Figure 9, with a C_L value of approximately 0.64. From that far right point in Figure 13 as the F-84 moves further inboard of the transport wingtip, the lift data decreases smoothly and appears to be coming to a plateau, where the F-84 would be fully enveloped by the downwash of the transport wing. The lift is actually negative at the minimum, $C_L \approx -0.25$.

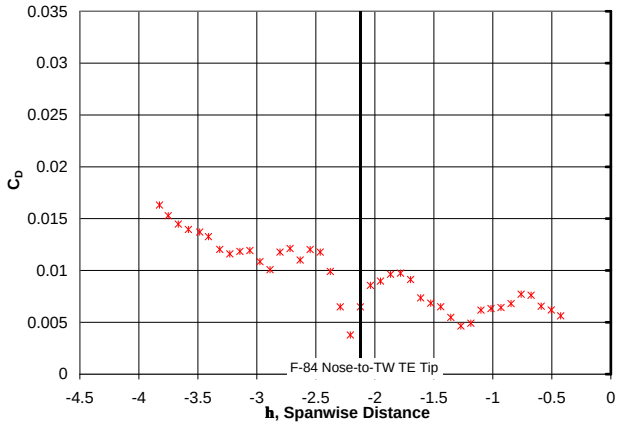

Figure 14: C_D vs. η, Spanwise Distance for Configuration Five

In Figure 14, the drag data for the F-84 in a towed configuration is presented for various spanwise locations. This data is more interesting than the lift data. The far right data point in Figure 14 coincides with the far left data point in Figure 10, with C_D values of approximately 0.005. As the F-84 continues to move inboard of the transport wingtip, the drag rises and falls twice with a sharp dip just after the nose of the F-84 passes the transport wingtip, $\eta \approx -2.25$ and $C_D \approx 0.004$. It then appears to plateau at about $C_D \approx 0.01$ for awhile, and then data rises to a maximum of $C_D \approx 0.015$ at $\eta = -3.8$. The drag data recorded for Configuration One in Figure 6 is still the largest at almost double the maximum recorded here.

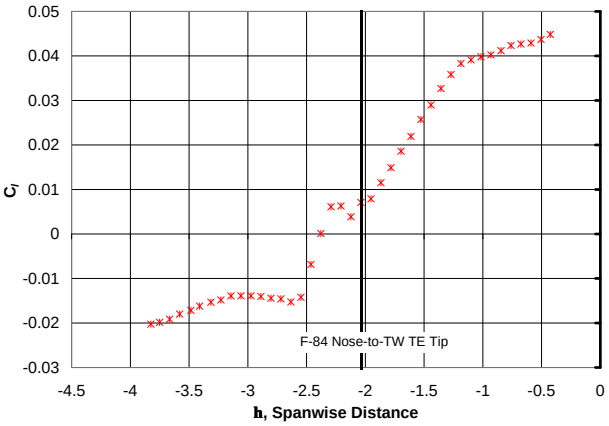

Figure 15: C_l vs. η, Spanwise Distance for Configuration Five

The rolling moment data for the F-84 in towed formation is presented in Figure 15. The rolling moment behavior is similar to the lift data in Figure 13; it is highest to the far right at $C_l \approx 0.045$ and lowest passing through the wingtip-to-wingtip plane at $C_l = 0.0$. If the F-84 passes spanwise from the beneficial upwash region to the non-beneficial downwash region of the transport wing trailing vortex, then it should be quite logical that the rolling moment would change direction. The velocity component shifts from upwash pushing on the inboard wing of the F-84 model to the outboard wing. Ultimately, in the more uniform downwash region the F-84 model should be trimmed and rolling moment should approximately equal zero. The rolling moment data appears to define two plateaus, one at $C_l \approx 0.04$ and the second at $C_l \approx -0.02$. Also, the curious dip in the drag data in Figure 14 is manifested here at the same spanwise location, $\eta = -2.25$, as a peak valued at $C_l \approx 0.008$. Having a discontinuity in the drag and roll data at the same point very close to the fuselage leads to the hypothesis that this is simply vortex-fuselage interaction with the circulatory motion being disrupted or transformed by the fuselage cylindrical shape.

In Figure 16, the L/D data for the F-84 to the

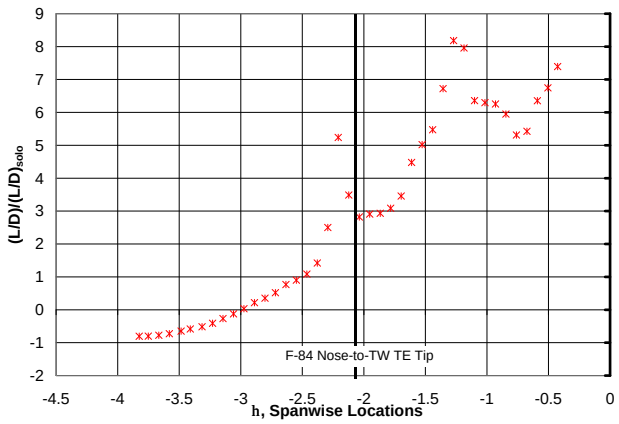

Figure 16: L/D vs. η, Spanwise Distance for Configuration Five

solo F-84 L/D is presented versus the various spanwise locations, η. The data seems to be driven by the interesting drag data in Figure 14, with the drag dips now manifested as L/D peaks at spanwise locations of $\eta \approx -1.25$ and $\eta \approx -2.25$. These excursions seem amplified in comparison to the drag data. The maximum flight performance benefit of $(L/D)/(L/D)_{solo} \approx 8$ is seen at the first peak, $\eta \approx -1.25$, and the second peak, $\eta = -2.25$, shows $(L/D)/(L/D)_{solo} \approx 5$. The $(L/D)/(L/D)_{solo}$ is a minimum at the far left data point, $\eta = -3.8$ at approximately -1.0.

Computational Aerodynamic Analysis

The computational aerodynamic analysis for compound aircraft transport flight presented here utilizes the vortex lattice method (VLM) for an incompressible and inviscid flow field about a finite wing. The goal of this effort was to develop a complement to the experimental data that would aid in understanding and interpreting the data, and also a simple tool for detailing a hitchhiker location of maximum aerodynamic benefit. All of the idiosyncracies seen in the experiments discussed previously cannot be accurately simulated because the VLM does not account for the real-life viscous effects present in the wind tunnel.

VLM yields consistently good results compared to empirical data for lift, but the classical near field induced drag calculation drag is somewhat lower than the minimum induced drag, for the case of an elliptic lift distribution, $\frac{C_{D_i}}{C_L^2} < \frac{1}{\pi AR}$. The error for this method presented in Kalman[7] is small, between 2-3%. The error would increase with wing sweep, Λ. Tulinius[8] proved that for the induced drag integrated from the bound vortex to be equal to the induced drag computed in the Trefftz plane; the panelling must be parallel and perpendicular to the free stream (i.e. unswept). Many have adopted an induced drag correcting scale factor based on the energy in the Trefftz plane. Kalman et al[7] define the ratio, $\frac{C_{D_{iw}}}{C_{D_{iV}}}$, where C_{D_iw} is the wake drag integral given in Equation 1 which sums the chordwise components of the normal force vector, and $C_{D_{iV}}$ is calculated by the downwash from VLM,

$$C_{D_i} = \frac{1}{2S}\int_{-s}^{s} c_l c\alpha_i dy. \qquad (1)$$

α_i does not vary with lift on an unswept wing in the same way it varies on a swept wing. Therefore Equation 1 is most easily evaluated in the Trefftz plane. This correcting scale factor method is commonly used for calculating the induced drag from the bound vortex, but it is not reliable near the tip, especially for variable leading edge angle planforms. Calculating the induced drag in the Trefftz plane is the usual method. Unfortunately for this work, we must separate the drag between components which cannot be done in the Trefftz plane. Fortunately, changes in the induced drag on a hitchhiker in formation flight are much greater than any error documented by sweeping panels, therefore the original method for calculating induced drag based on the downwash at the bound vortex is used here to determine trends in formation flight as observed in the wind tunnel.

Full simulation of the aerodynamic problems of interest here would require treatment of the viscous effects which surely become important as the wings of the mothership and hitchhiker come close together, and the wake deformation and vortex core become important. This would necessitate using a three-dimensional, Navier-Stokes code and elaborate gridding techniques. Such an effort was deemed outside the scope of this work.

Compound Aircraft Transport Vortex Lattice Method

A simple baseline VLM code was extended to treat CAT systems using the techniques described in Bertin and Smith's *Aerodynamics for Engineers*[5]. The code required the axial location (x-direction) of the leading and trailing edge root and tip as well as the spanwise location (y-direction) of the root and tip for the wing planform. This coordinate system

was referenced with respect to a plane of symmetry originating at the leading edge centerline. Also input are the number of spanwise (NSPAN) and chordwise (NCHRD) divisions to create a lattice structure of N (NSPAN by NCHRD) trapezoidal panels.

With this basic information, one-dimensional arrays are created for the x, y, and z locations of the panels, horseshoe vortices, and control points in the plane of symmetry. The arrays are then sent to a subroutine, VHORSE, twice to calculate the appropriate influence coefficient matrix, $\vec{C}_{m,n}$ from Equation 1, based on the Biot-Savart Law. VHORSE is called once with the given coordinates and then again with the mirrored coordinates ($Y = -Y$) to incorporate the total influence at each control point from the $2N$ panels. Then, applying the flow tangency boundary condition at the panel $\frac{3c}{4}$ or control point the circulation for each panel is solved through the Gaussian Elimination. The known circulations are summed and the Kutta-Joukowski theorem applied to determine the sectional and total lift and pitching moment coefficient slopes. The output consists of the wing planform and panel geometry, as well as the circulation of each panel with the spanwise lift distribution and the total coefficient slopes, C_{L_α} and C_{M_α} per radian.

The modifications for the CAT model, here, began with the geometric reconstruction of the VLM code to accept multiple aircraft, which were represented as planar, flat, surfaces without camber. The system origin remained the same at the mothership leading edge centerline. Each additional aircraft or hitchhiker was input based on its individual origin at the hitchhiker leading edge centerline. Geometric symmetry is a requirement of each aircraft. The location of the hitchhiker is then referenced to the mothership by inputting the coordinates of the hitchhiker origin with respect to the mothership origin in terms of her coordinate system. The layout for the original VLM and the VLM modified for CAT flight is given in Figure 17.

The accuracy of the method and code was first proven by moving two identical aircraft far apart with the code yielding the same results, for an unswept wing of aspect ratio 4.0 and the well-known Warren 12 planform for a swept wing.

The wind tunnel data analyzed aerodynamic trends in CAT flight through lift-to-drag ratio, but the original VLM code only calculates lift and not drag. So, the technique described in the previous section for calculating induced drag was applied. The code determines the circulation for each panel

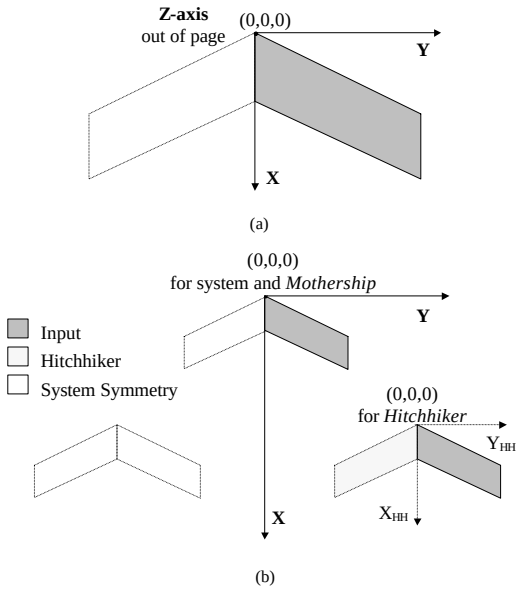

Figure 17: Coordinate System for (a) the Original VLM and (b) the VLM Modified for CAT Flight

in the CAT system, but induced drag requires the downwash, $w_{m,n}$, of each panel as well. By changing the influence coefficient matrix using the known circulations to solve for panel downwash, the induced drag can be calculated by the rearranged Kutta-Joukowski theorem. So the subroutine, VHORSE, was called twice more (4 times total) with the modification for r in the Biot-Savart Law. This changed only the axial location sent to the subroutine making it the center of the bound finite horseshoe vortex segment, the panel quarter chord. The downwash for each panel was determined based on the velocity induced by all other system horseshoe vortices. These values can be integrated over the wing to yield sectional and total induced drag coefficients. Note, the total induced drag slope would have units of $C_{Di_{\alpha^2}}$ per radian squared; recall $C_{D_i} \propto C_L^2$. The proof of accuracy for induced drag has much less data available for comparison. The Kalman et. al. paper[7] documented a $\frac{C_{D_i}}{C_L^2} = 0.155375$ value for an unswept wing with an aspect ratio of 2.0 and VLM CAT yielded $\frac{C_{D_i}}{C_L^2} = 0.15537$; this is very good agreement. To test for swept wings the comparison relied on the fact that two aircraft (mothership and hitchhiker) of the same geometry far apart should have the same induced drag values.

VLM CAT Compared to Wind Tunnel Data

To make a reasonable comparison between the VLM CAT results and the wind tunnel data, a proper lift-to-drag ratio needed to be determined for the VLM CAT results. The VLM supplies a C_{L_α} and a $C_{Di_{\alpha^2}}$. First, an estimate for parasite drag, C_{D_o} was calculated following two different methods; total drag is $C_D = C_{D_o} + C_{D_i}$ plus drag due to compressibility effects or wave drag which would be negligible at the speeds considered here. Method One followed the techniques presented in Shevell's *Fundamentals of Flight*[10]. This requires the summation of C_{D_o} for each aircraft component based on wetted area, S_{wet}, skin friction as a function of Reynolds Number, and pressure effects due to thickness. It can be reasonably assumed that the wing is the major lift-producing component on an aircraft, thus an L/D ratio from the VLM CAT should compare more favorably to the wind tunnel data by simply adding the parasite drag due to the majority of the F-84, the fuselage and wing.

Method Two assumed a point of maximum performance for the hitchhiker at $C_L = 0.48$ (the $C_{L_{solo}}$ in the wind tunnel), which is theoretically when $C_{D_o} = C_{D_i}$. Parasite drag is typically considered invariant with a constant-Reynolds number flow field, so C_{D_o} of the F-84 was chosen to equal C_{D_i} of the F-84 when far from the transport wing, $C_{D_o} \approx 0.01$.

Next, since the coefficients are output from VLM as slopes with respect to an angle of attack, α, so α from the wind tunnel tests need to be specified. Recall earlier comments about the difficulty in measuring accurately the angle of attack; a reference solo C_L was chosen *in lieu* of an α. So, the reference solo hitchhiker $C_{L_{solo}} = 0.48$ was applied to the VLM output C_{L_α} to determine a corresponding flight α,

$$C_{L_\alpha} = \frac{dC_L}{d\alpha} \Longrightarrow \alpha = \frac{C_{L_{solo}}}{C_{L_\alpha}}.$$

One more value must be defined before the VLM CAT and wind tunnel data can be compared. The wind tunnel data defined a lift-to-drag ratio based on the solo values of the hitchhiker, $(L/D)/(L/D)_{solo}$. The value in the wind tunnel data was $(L/D)_{solo} = 18$. But, this value is not the same for VLM CAT, since only the wing geometries were implemented and the total viscous drag effects were not accurately simulated, the value for VLM CAT is $(L/D)_{solo} = 15.7$.

The number of chordwise and spanwise panels for the mothership and the hitchhiker in VLM CAT were determined mainly through a simple grid refinement study comparing the lift curve slope, C_{L_α}, between the original VLM and VLM CAT with the aircraft far apart. The resulting spanwise by chordwise (NSPAN X NCHRD) panelling selected was 20 X 5 for the mothership and 25 X 5 for the hitchhiker based on symmetry of the individual aircraft[4]. These values were chosen from the grid refinement study and computational time, with an error $\leq 3.0\%$ being considered adequate. A diagrammatic view of the panelling applied to the mothership and hitchhiker planforms used here is in Figure 18.

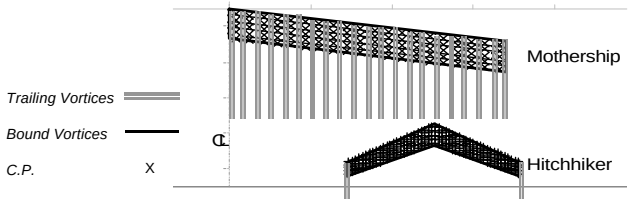

Figure 18: VLM CAT Panelling Presented in Configuration Five: *Towed Formation* (Axisymmetric)

The VLM CAT results demonstrate similar trends in aerodynamic benefits as for CAT flight in the wind tunnel. VLM CAT was modelled for the three distinct formations: *wingtip-docked flight, close-formation flight,* and *towed-formation flight*, studied in the wind tunnel. To clearly show the comparison between the wind tunnel data and VLM CAT results, only one vertical location, ζ, is presented for each configuration. Configuration One is at the wingtip-to-wingtip location and the subsequent locations progress the hitchhiker further downstream from the mothership. VLM CAT results, are distinguished from experimental data by dashed or solid lines connecting the points.

Configuration One: *Wingtip-Docked CAT Flight*

The VLM CAT results are plotted in the same method as the experimental wind tunnel data. The C_L, C_D, and L/D data output from VLM CAT are plotted versus the spanwise or gap separation, η, between the wingtip of the F-84 and the wingtip of the transport wing in Figures 19 through 21. The symbols on the connecting lines correspond to the same various vertical locations for the F-84 wing above and below the transport wing as the wind tunnel data. Also, like the wind tunnel data the transport wing, is fixed and the F-84 is moved relative to her. The L/D ratio data in Figure 21 for dif-

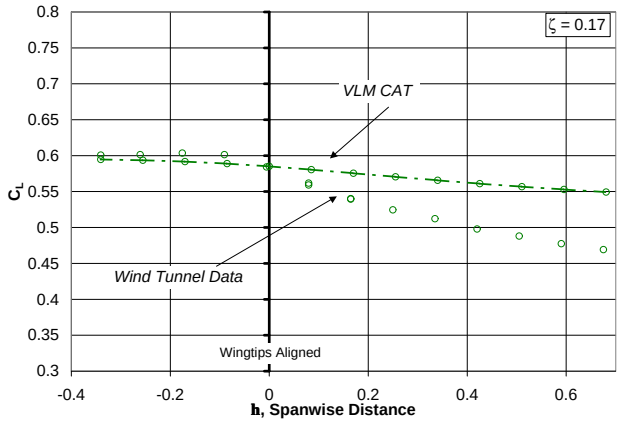

Figure 19: Configuration One: *Wingtip-Docked Formation*, $\xi = 0.0$, VLM CAT Compared to Experimental Data; C_L vs. η, Spanwise Distance

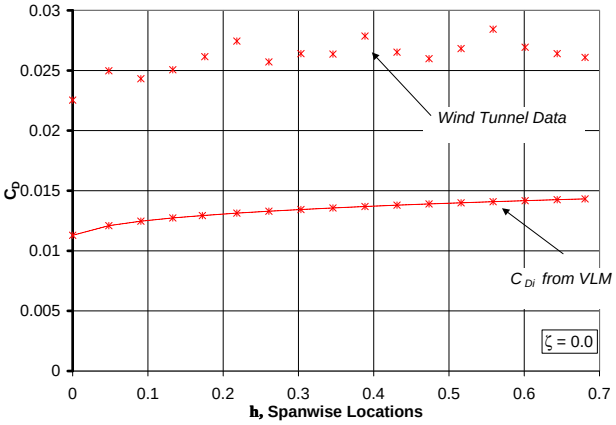

Figure 20: Configuration One: *Wingtip-Docked Formation*, $\xi = 0.0$, VLM CAT Compared to Experimental Data; C_D vs. η, Spanwise Distance

fering parasite drag calculations are distinguished with a dashed line for $C_{D_o} = 0.01$ and solid line for $C_{D_o} = 0.018$.

The VLM CAT lift data compared to the wind tunnel lift data, in Figure 19, with the mothership wingtip and hitchhiker wingtip in-plane, $\zeta = 0.0$, shows generally good agreement. In Figure 20, the VLM CAT induced drag is plotted with the wind tunnel total measured drag, and the offset is about 0.01. Referring to Figure 21, the offset in $(L/D)/(L/D)_{solo}$ data between induced and total drag must be closest to the value calculated with a parasite drag based on the planform of the F-84 wing and fuselage, i.e. $C_{D_o} = 0.018$. Recall that the drag

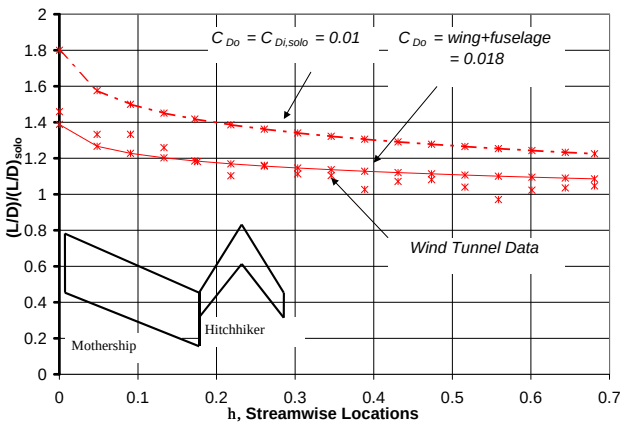

Figure 21: Configuration One: *Wingtip-Docked Formation*, $\xi = 0.0$, VLM CAT Compared to Experimental Data; L/D vs. η, Spanwise Distance

for the configuration in Figure 6 was quite invariant. One can thus conclude that the aerodynamic benefit is driven by the inviscid force, lift. VLM can predict forces in an inviscid flow field very well.

The maximum aerodynamic benefits for this configuration are at the wingtip-to-wingtip location, $\eta = 0.0$. The performance increase is 60–80% for the VLM CAT results with the smaller parasite drag value and within the same range predicted by the wind tunnel data, 20 – 40%, with larger value of parasite drag. Though only one vertical location is presented for clarity, the VLM CAT results coincide for all points outboard of the wingtip-to-wingtip location, $\eta = 0.0$. So, an important differing point is that the wind tunnel data shows an overall increase in aerodynamic benefit for a vertical position slightly below the transport wing, but VLM CAT does not predict this.

Configuration Two: *Close Formation CAT Flight*

In Figures 22 through 24, the VLM CAT results and wind tunnel data for C_L, C_D, and $(L/D)/(L/D)_{solo}$ in Configuration Two, close formation, is plotted versus the spanwise or gap separation, η. The data is presented for a vertical location of the F-84 further above at $\zeta = 0.34$. This change in ζ is because Figure 25 is depicting a different range of $(L/D)/(L/D)_{solo}$ than Figure 24.

The VLM CAT results for the outboard locations of the hitchhiker wingtip, $\eta > 0.0$, support the wind tunnel data trends well. Inboard of the transport

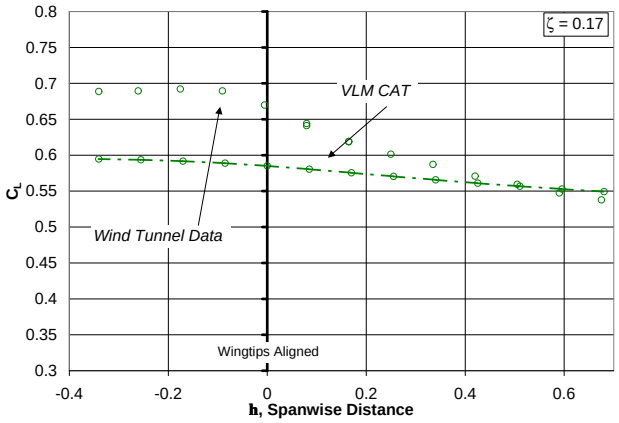

Figure 22: Configuration Two: *Close Formation Flight*, $\xi = 3.0$ VLM CAT Compared to Experimental Data; C_L vs. η, Spanwise Distance

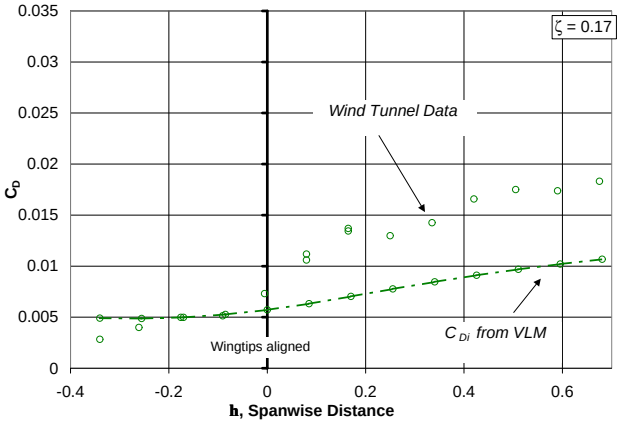

Figure 23: Configuration Two: *Close Formation Flight*, $\xi = 3.0$ VLM CAT Compared to Experimental Data; C_D vs. η, Spanwise Distance

wingtip, $\eta < 0.0$, the VLM CAT lift results in Figure 22 diverge from the test data, but do, in general, support the overall increasing trend of the wind tunnel data. Figure 23 plots the wind tunnel data and the VLM CAT results in drag for a vertical position of $\zeta = 0.17$. Only the induced drag, which is directly from the VLM CAT calculations is presented for comparison, and it follows the trend of the wind tunnel data. For an F-84 position inboard of the transport wingtip, $\eta < 0.0$, the induced drag coincides closely with the wind tunnel data for a small range between $\eta \approx -0.1$ and $\eta \approx -0.25$. For η smaller than -0.25 the VLM CAT induced drag overpredicts the data and for η larger than 0.0 the VLM

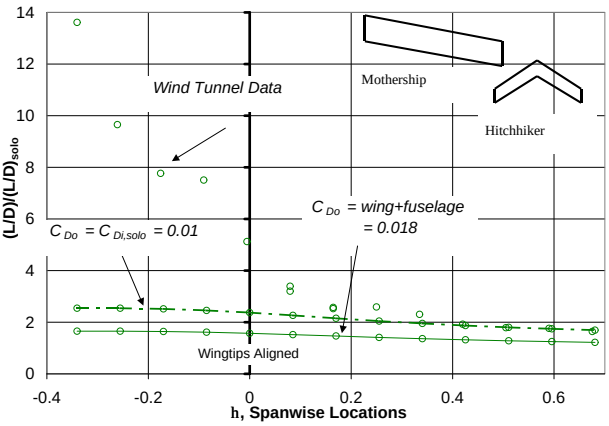

Figure 24: Configuration Two: *Close Formation Flight*, $\xi = 3.0$ and $\zeta = 0.17$, VLM CAT Compared to Experimental Data; L/D vs. η, Spanwise Distance: Large L/D Scale

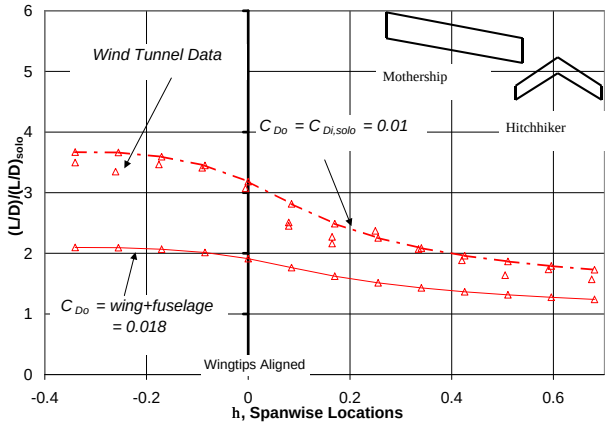

Figure 25: Configuration Two: *Close Formation Flight*, $\xi = 3.0$ and $\zeta = 0.34$, VLM CAT Compared to Experimental Data; L/D vs. η, Spanwise Distance: Small L/D Scale

CAT data underpredicts the data.

The lift behavior is revisited in Figure 24 when the $(L/D)/(L/D)_{solo}$ VLM CAT results inboard of the transport wingtip, $\eta = 0.0$, clearly do not pick up the large benefits in performance seen in the data. The wind tunnel data measured benefits up to 1100%, while the VLM CAT results only yield benefits about 100–300%. Figure 10 of the wind tunnel drag data shows a large reduction in drag for hitchhiker wingtip locations inboard of the mothership wingtip, while the lift data in Figure 9 is very simi-

lar to that in Figure 5. This being the case, it is clear that reduction in drag must be the driver in increasing the aerodynamic benefits, and since VLM cannot accurately predict benefits caused by viscous effects, then the results in Figure 24 are expected. The VLM CAT results like the wind tunnel results show a significant increase in flight performance benefit from close formation flight compared to wingtip-docked. VLM CAT shows a rise in aerodynamic benefit from $20-40\%$ to $\sim 100-300\%$ benefit. In Figure 24, the VLM CAT results with the smaller parasite drag ($C_{D_o} \approx C_{D_{i,solo}}$) are more comparable to the wind tunnel data. Figures 24 and 25 highlight different ranges of wind tunnel $(L/D)/(L/D)_{solo}$ data. The VLM CAT results do not pick up the benefits in the larger range $(0.0 \leq (L/D)/(L/D)_{solo} \leq 14.0)$ in Figure 24, but do in the smaller range $(0.0 \leq (L/D)/(L/D)_{solo} \leq 6.0)$ in Figure 25.

Configuration Five: *Towed Formation CAT Flight*

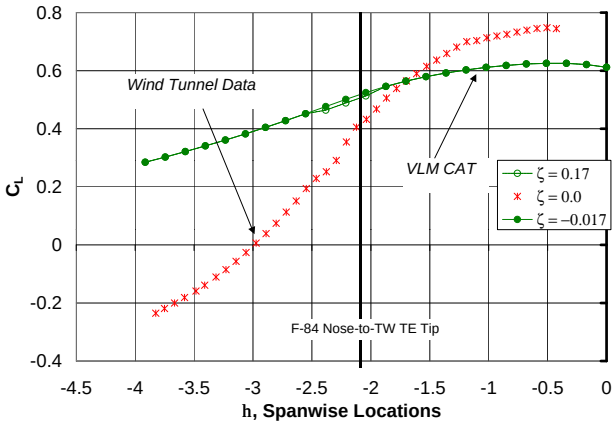

Figure 26: Configuration Five: *Towed Formation Flight*, $\xi = 10.0$, VLM CAT Compared to Experimental Data; C_L vs. η, Spanwise Distance

In VLM, trailing vortices cannot intersect a control point, and the fineness of the grid necessary in CAT made it difficult for the trailing horseshoe vortices of the mothership not to intersect the control points of hitchhiker when the hitchhiker is inboard of the mothership wingtip. Thus, the simple expedient used here was to separate the mothership and hitchhiker vertically, slightly.

The VLM CAT results for lift are presented in Figure 26 and like the previous VLM CAT lift data in Configuration Two, the inboard locations of the

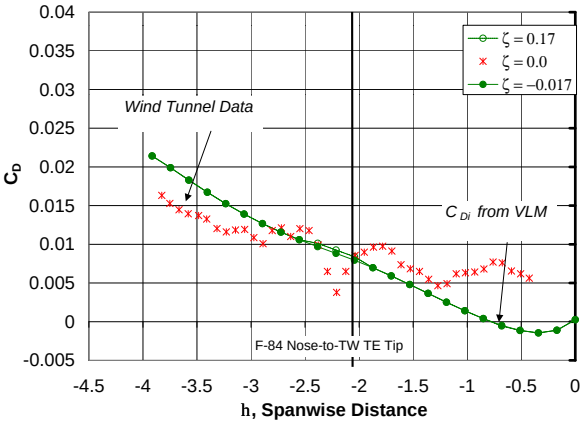

Figure 27: Configuration Five: *Towed Formation Flight*, $\xi = 10.0$, VLM CAT Compared to Experimental Data; C_D vs. η, Spanwise Distance

F-84, $\eta < 0.0$, the VLM CAT data diverges from the wind tunnel data. But again, the overall trend is duplicated, the lift decreases on the F-84 as it is moved into a downwash region inboard of the transport wingtip. Oddly, the VLM CAT induced drag data presented in Figure 27 with the wind tunnel total drag, is nearly identical. The $(L/D)/(L/D)_{solo}$

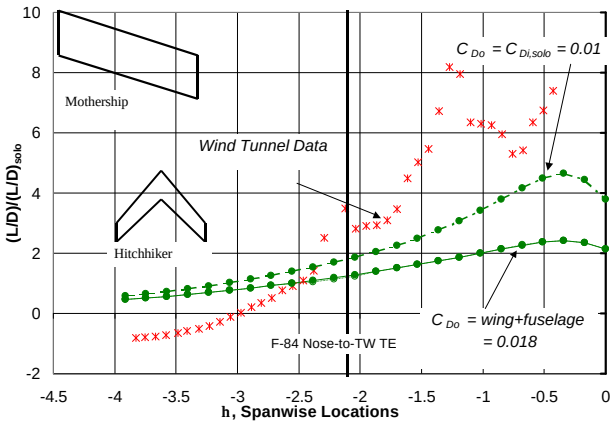

Figure 28: Configuration Five: *Towed Formation Flight*, $\xi = 10.0$, VLM CAT Compared to Experimental Data; L/D vs. η, Spanwise Distance

at the far right of Figure 28 is the highest. Using $C_{D_o} = 0.018$, $(L/D)/(L/D)_{solo} \approx 2.3$ and then falls smoothly as the hitchhiker wingtip moves inboard of the mothership wingtip to a minimum at $(L/D)/(L/D)_{solo} \approx 0.5$. The wind tunnel data rises above and below the maximum and minimum values from VLM CAT. It is important to mention, VLM

CAT cannot model the fuselage of the F-84, therefore if the spikes in wind tunnel results are due to fuselage-vortex interaction, then VLM CAT would not predict these effects.

Summary and Conclusions

The wind tunnels experiments showed that the close formation, Configuration Two, yielded the greatest ($\sim$ 1100%) aerodynamic benefit through large reductions in drag. The wingtip-docked configuration showed aerodynamic benefits (20-40%) when the F-84 and transport wing were tip-to-tip based on the lift force. The towed formation showed aerodynamic benefits ($\sim$ 800%) driven by drag almost as large as the close formation. However, this is not the whole story; other factors must be considered to conclude what is the best location for a hitchhiker with respect to the mothership. As mentioned previously, the issue of hitchhiker control is a factor in feasibility; that is why the roll data is presented as well. The large magnitude of the velocities close to a wingtip trailing vortex could render a smaller hitchhiker uncontrollable, particulary in roll due to the circulatory nature of a vortex.

Similar data was plotted for the transport wing for lift, drag, lift-to-drag ratio, but due to the large size of the transport wing compared to the F-84 model, there was relatively little change in the forces and moments on the transport wing as the F-84 model was moved. This is emphasized by the flow visualization, which saw an unaffected trailing wingtip vortex from the transport wing when the F-84 model was moved in close to her wingtip. The transport wing did see benefits and not losses in aerodynamic performance, 20 – 80 %, but this is small compared to the corresponding performance increases in the F-84 (400 – 1100 %). All of the transport wing data is in Magill[4].

The VLM CAT results model the general trends of the wind tunnel data well. The aerodynamic benefits in the wind tunnel experiments that derived from viscous force or drag reduction are not predicted as well as the inviscid aerodynamic benefits. The VLM CAT results in Figures 19 and 21 are almost identical to the wind tunnel data, which showed only strong variation in lift and not in drag. It is clear that the correct choice or method in calculating parasite drag could be an important factor in determining the correct total drag for VLM CAT and wind tunnel comparison. Parasite drag is complicated to calculate and is usually estimated by subtracting induced drag and wave drag (which can be reasonably calculated) from the measured total drag. Other issues associated with the complex flow field of wingtip-docked and formation flight could negate the assumption of invariant parasite drag. For instance, the flow field in the small gap when the two aircraft are close together might cause boundary layer separation or thickening, both varying the values of skin friction from that based on free-stream conditions[6]. Another assumption in this VLM is that of a flat wake, all lift is produced on the quarter chord of each panel. Flow fields of this nature with aircraft flying close behind one another would likely have substantial deformation in their wakes, and incorporating the wake deformation with respect to the freestream would undoubtedly yield results more comparable to the wind tunnel data.

At some locations in the drag data, the VLM CAT induced drag was greater than the total wind tunnel drag and at other locations, the VLM CAT induced drag was greater than the total wind tunnel drag. So VLM CAT is sometimes overpredicting and other times underpredicting induced drag. Viscosity cannot be modelled in VLM by its formulation, only a full three-dimensional Navier-Stokes code could describe all the viscous effects. But, regardless of the uncertainty in calculating total drag and associated assumptions, the VLM CAT program does supply valuable knowledge and insight in quickly determining the aerodynamic benefits for CAT flight in terms of position of the hitchhiker with respect to the mothership and in terms of different geometries or planforms.

In conclusion the most aerodynamically beneficial location for a hitchhiker with respect to a mothership is aft, off-center (below), and slightly inboard of the mothership based on the wind tunnel testing. This is congruent with the flight test data of the Autonomous Flight Formation Project which shows a region of maximum upwash, thus maximum benefit, inboard and beneath the lead aircraft's trailing wingtip vortex[11].

Acknowledgments

This work was supported by the Lockheed Martin Aerospace Coorporation.

References

[1] Anderson, C.E. "Bud". "Dangerous Experiments". *Flight Journal.* Pp. 65-72, December 2000.

[2] Erickson, B.A., phone conversation, June 2001.

[3] Strnad, Frank. "Project 'Tom-Tom'". AEROPHILE. pp. 161-164, 1977.

[4] Magill, Samantha A. "Compound Aircraft Transport: A study of Windtip-Docked Flight and Close Formation Flight". Dissertation on Partial Fulfillment for the Degree of Doctorate of Philosophy in Aerospace Engineering, Virginia Polytechnic Institute and State University, Blacksburg, VA 24061, May 2002.

[5] Bertin, John J. and Smith, Michael L. *Aerodynamics for Engineers.* Prentice Hall, Englewood Cliffs, NJ 07632, second edition, 1989.

[6] Blake, William B. and Gingras, David R. "Comparison of Predicted and Measured Formation Flight Interference Effects". *AIAA*, (2001-4136), 2001.

[7] Kalman, T.P. et. al. "Spanwise Distribution of Induced Drag in Subsonic Flow by the Vortex Lattice Method". *Journal of Aircraft*, Nov.-Dec. 1970.

[8] Tulinius, J. et. al. "Theoretical Prediction of Airplane Stability at Subcritical Speeds". *NACA*, (CR-132681), August 1975.

[9] Karamcheti, Krishnamurty. *Principles of Ideal-Fluid Aerodynamics*. Krieger Publishing Company, Malabar, FL, second edition, 1980.

[10] Shevell, Richard S. *Fundamentals of Flight*. Prentice Hall, Englewood Cliffs, NJ 07632, second edition, 1989.

[11] Iannotta, Ben. "Vortex Drag Flight Research Forward". *Aerospace America*. March 2002, pp. 26 – 30.